

A lattice Boltzmann model for multiphase flows with large density ratio

H.W. Zheng, C. Shu ^{*}, Y.T. Chew

Department of Mechanical Engineering, National University of Singapore, Singapore 119260, Singapore

Received 26 April 2005; received in revised form 13 February 2006; accepted 16 February 2006

Available online 17 April 2006

Abstract

A lattice Boltzmann model for simulating multiphase flows with large density ratios is described in this paper. The method is easily implemented. It does not require solving the Poisson equation and does not involve the complex treatments of derivative terms. The interface capturing equation is recovered without any additional terms as compared to other methods [M.R. Swift, W.R. Osborn, J.M. Yeomans, Lattice Boltzmann simulation of liquid–gas and binary fluid systems, *Phys. Rev. E* 54 (1996) 5041–5052; T. Inamuro, T. Ogata, S. Tajima, N. Konishi, A lattice Boltzmann method for incompressible two-phase flows with large density differences, *J. Comput. Phys.* 198 (2004) 628–644; T. Lee, C.-L. Lin, A stable discretization of the lattice Boltzmann equation for simulation of incompressible two-phase flows at high density ratio, *J. Comput. Phys.* 206 (2005) 16–47]. Besides, it requires less discrete velocities. As a result, its efficiency could be greatly improved, especially in 3D applications. It is validated by several cases: a bubble in a stationary flow and the capillary wave. The numerical surface tension obtained from the Laplace law and the interface profile agrees very well with the respective analytical solution. The method is further verified by its application to capillary wave and the bubble rising under buoyancy with comparison to other methods. All the numerical experiments show that the present approach can be used to model multiphase flows with large density ratios.

© 2006 Elsevier Inc. All rights reserved.

Keywords: Lattice Boltzmann; Large density ratio

1. Introduction

Multiphase and multi-component flows have been given many attentions for years since they are ubiquitous in both the nature and industry. To model them, two main issues, surface tension force modeling and interface recording, have to be considered. These two factors are often mixed together. The treatment of these two factors is especially difficult for flows with large density ratio.

Conventionally, the multiphase and multi-component flows are simulated by solving a set of Navier–Stokes equations coupled with an equation to track or capture the interface, which may encounter some numerical

^{*} Corresponding author. Tel.: +65 6874 6476; fax: +65 6779 1459.

E-mail address: mpeshuc@nus.edu.sg (C. Shu).

difficulties in treatment of topological deformation of interface breaking and coalescing. Among the approaches, VOF [7,26,23,32,21] and level set method [20,27] are applied extensively. Both of them solve a scalar transport equation in the Eulerian frame. In fact, VOF method does not track the interface itself. Instead, it, tracks the volume fraction of each phase or component [21]. The interface is reconstructed from the values of volume fraction. This may imply that it would be complicated for VOF to be extended to the three-dimensional case. Besides, most of VOF interface reconstruction schemes only have the first order of accuracy. For the level set method, it uses the level set function to store the information of the interface. The advantage is that the level set function varies smoothly across the interface while the volume fraction is discontinuous. Besides, the curvature can be easily evaluated from the level set function. However, the level set method requires a re-initialization procedure to keep the distance property when large topological changes occur around the interface. This may violate the mass conservation for each phase or component.

Recently, the lattice Boltzmann method became a promising tool to simulate the incompressible viscous flows [4]. It is very simple in the sense that it only involves a series of collision and stream steps. Unlike the traditional CFD, it does not solve the differential equation. Besides, it is relatively easy to set the non-slip boundary condition for complex geometry. Thus, it is a natural demanding to develop a lattice Boltzmann method to model the multiphase flow. In fact, in the lattice Boltzmann context, there are several models developed for multiphase and multi-component flows during the last twenty years. They are Rothman and Keller's color method [24], Shan et al.'s potential method [28], Swift et al.'s free energy method [29] and He et al.'s method [6]. All these methods regard the interface as a transition layer (diffuse interface). The color and potential methods do not explicitly describe the evolution of the interface. They regard the region with non-zero gradient of density difference as the interface. In He et al.'s method, the physics of the interface capturing equation is not clear. Besides, the mobility is related to the density and cannot be flexibly chosen. In contrast, the free energy method captures the interface by solving a convection–diffusion equation. A distribution function is designed to solve this equation. By using the Chapman–Enskog expansion, the distribution function will recover the modified Cahn–Hilliard equation which is an evolution equation for the interface. This equation evolves the order parameter (for example, density difference) which is used to distinguish different phases or components. In this sense, the order parameter is quite similar to the indicator of the traditional volume tracking method such as VOF. Usually, the density ratio cannot be very large due to numerical instability. To overcome this difficulty, Inamuro et al. [8] proposed a model, based on the free energy method for multiphase flows with large density ratio. But their method shows some deficiencies. That is, like VOF method [26,19] and level set method [27], the pressure correction is applied to enforce the continuity condition after every collision-stream step. The projection step would reduce the efficiency of the method greatly. Besides, the cut-off value of the order parameter and the surface tension coefficient are not analytically given. In fact, it is not easy to give the cut-off value because sometimes the order parameter may go beyond the range given by cut-off value. It may give rise to some non-physical disturbances in some cases even though the divergence of velocity field is zero (such as in the shear flow). In this sense, it may not be accurate for some incompressible flows although the projection procedure is employed to secure the incompressible condition. Lee and Lin [18] developed a stabilized scheme of discrete Boltzmann equation [6] for multiphase flows with large density ratio. They used another pressure update scheme to stabilize the LBE method and adopted the idea of Jamet et al. [10] about different features of the different pressure tensor forms. However, it suffers the same problem as He et al. [6] that it still does not completely recover the lattice Boltzmann equation for interface to the Cahn–Hilliard equation. Besides, at different steps, the discretization forms are different. Thus, the implementation is quite complex and the efficiency may be very low since the process involves discretization of many first order and second order derivatives. We can easily find that all the existing methods did not completely recover the lattice Boltzmann equation for interface to the Cahn–Hilliard equation. The efficiency is also not good. In addition, all the methods use the nine bits discrete velocity model in 2D interface capturing and fifteen or even more bits discrete velocity model in 3D interface capturing. To solve these problems, a method is proposed in this paper. It recovers the lattice Boltzmann equation to the Cahn–Hilliard equation without any additional terms and it can keep the Galilean invariance property. In addition, the potential form of the surface tension related term is applied to reduce the spurious currents. Similar to the work of Lee and Lin [18], the large density difference is incorporated in the interface capturing equation. Thus, it can be used to model the multiphase flows with large density ratio which can be beyond 1000.

The paper is organized as follows. The new method with interface capturing is proposed in Section 2. Then it is verified in Section 3. Some test cases will be applied to validate the method. The present results will also be compared with those of other methods, such as VOF and Takada's method. Numerical results show that our method can be used to model multiphase flows with large density ratio as well as capture the accurate position of the interface. Finally, the conclusion will be drawn.

2. Methodology

Here, we consider a flow with two fluids or phases which have different densities. Hereafter, for the sake of convenience, the low density and high density are noted as ρ_L and ρ_H respectively. The flow can be described by the Navier–Stokes equations and an interface evolution equation as [9,14,31]

$$\frac{\partial n}{\partial t} + \vec{\nabla} \cdot (n\vec{u}) = 0, \quad (1)$$

$$\frac{\partial(n\vec{u})}{\partial t} + \vec{\nabla} \cdot (n\vec{u}\vec{u}) = -\vec{\nabla} \cdot P + \mu \vec{\nabla}^2 \vec{u} + \vec{F}_b, \quad (2)$$

$$\frac{\partial \phi}{\partial t} + \vec{\nabla} \cdot (\phi \vec{u}) = \theta_M \nabla^2 \mu_\phi. \quad (3)$$

Here, μ_ϕ is the chemical potential, θ_M is the mobility, P is the pressure tensor, \vec{F}_b is the body force, and n, ϕ are defined as [31]

$$n = \frac{\rho_A + \rho_B}{2}, \quad \phi = \frac{\rho_A - \rho_B}{2},$$

where ρ_A and ρ_B are the density of fluid A and fluid B respectively. They may be ρ_L or ρ_H and depend on the initial conditions.

2.1. The interface capturing equation

The interface capturing is modeled by a convective Cahn–Hilliard equation [3]. This equation has been investigated by many researchers [30,15]. However, they did not completely recover the correspondent LBE to the convective Cahn–Hilliard equation. For example, as shown in [30], it recovers the equation below with the second order of accuracy

$$\partial_t \phi + \vec{\nabla} \cdot (\phi \vec{u}) - \left(\tau - \frac{1}{2} \right) \delta [\vec{\nabla}^2 (\Gamma \mu_\phi) + \vec{\nabla} \vec{\nabla} : (\phi \vec{u}\vec{u}) + \partial_i \vec{\nabla} \cdot (\phi \vec{u})] + O(\delta^2) = 0. \quad (4)$$

It is obvious that the above equation has two additional terms. In fact, up to now, this problem remains in all LB methods. For example, in the work of Inamuro et al. [8], the governing equation is replaced as

$$\frac{\partial \phi}{\partial t} + \vec{\nabla} \cdot (\phi \vec{u}) = \vec{\nabla} \cdot (\vec{\nabla} \cdot P), \quad (5)$$

where P is the pressure tensor. This equation is quite similar to Eq. (3). However, it also has the additional term $\partial_i \vec{\nabla} \cdot (\phi \vec{u})$ so that this method lacks Galilean invariance. Besides, its physical background is not very clear. Similarly, the governing equation in [18] is

$$\frac{\partial \rho}{\partial t} + \vec{\nabla} \cdot (\rho \vec{u}) = \vec{\nabla} \cdot [\tau (\vec{\nabla} p^{\text{therm}} - \vec{\nabla} p^{\text{hydro}})], \quad (6)$$

where p^{therm} and p^{hydro} are the thermodynamic pressure and hydrodynamic pressure respectively. This equation also has some spurious terms as compared with Eq. (3). Besides, the mobility is related to the density in this model. Thus, it cannot be easily modified physically.

In order to recover Eq. (3), we adopted a modified lattice Boltzmann equation [16]

$$g_i(\vec{x} + \vec{c}_i \delta, t + \delta) = g_i(\vec{x}, t) + (1 - q)[g_i(\vec{x} + \vec{c}_i \delta, t) - g_i(\vec{x}, t)] + \Omega_i, \quad (7)$$

with BGK approximation of the collision term [2]

$$\Omega_i = \frac{g_i^{(0)}(\vec{x}, t) - g_i(\vec{x}, t)}{\tau_\phi}, \quad (8)$$

where g_i is the distribution function, τ_ϕ is the dimensionless single relaxation time, \vec{c}_i is the lattice velocity, q is a constant coefficient. It will reduce to the conventional lattice Boltzmann equation when q is set to be one.

The macroscopic variable (order parameter) ϕ is evaluated by

$$\phi = \sum_i g_i. \quad (9)$$

With these definitions,

$$\sum_i g_i = \sum_i g_i^{(0)} = \phi, \quad (10)$$

$$\sum_i g_i^{(0)} c_{ix} \equiv \frac{\phi}{q} u_x, \quad (11)$$

$$\sum_i g_i^{(0)} c_{ix} c_{i\beta} = \Xi_{x\beta}. \quad (12)$$

By Chapman–Enskog expansion, we can obtain

$$\begin{aligned} \partial_t \phi + \vec{\nabla} \cdot (\phi \vec{u}) + \delta \left[\left(\frac{1}{2} - \tau_\phi \right) (\partial_t^2 \phi + \partial_t \vec{\nabla} \cdot (\phi \vec{u})) + \left(\frac{-2\tau_\phi q + 1}{q} + \tau_\phi - \frac{1}{2} \right) \partial_t \vec{\nabla} \cdot (\phi \vec{u}) \right] \\ + \left(\frac{q}{2} - \tau_\phi q^2 \right) \delta \vec{\nabla} \vec{\nabla} : \Xi + O(\delta^2) = 0. \end{aligned}$$

As indicated (Eq. (B2)) in the Appendix of [30], the first and second terms in the bracket of above equation is of higher order and can be neglected. So, the equation above can be written as

$$\partial_t \phi + \vec{\nabla} \cdot (\phi \vec{u}) + \left(\frac{q}{2} - \tau_\phi q^2 \right) \delta \vec{\nabla} \vec{\nabla} : \Xi + \left(\frac{-2\tau_\phi q + 1}{q} + \tau_\phi - \frac{1}{2} \right) \delta \partial_t \vec{\nabla} \cdot (\phi \vec{u}) + O(\delta^2) = 0.$$

Thus, we can show that if the equilibrium distribution function satisfies

$$\Xi_{x\beta} = \Gamma \mu_\phi \delta_{x\beta}, \quad (13a)$$

and the coefficient q is set to be

$$\left(\frac{-2\tau_\phi q + 1}{q} + \tau_\phi - \frac{1}{2} \right) = 0$$

which further gives

$$q = \frac{1}{\tau_\phi + 0.5}, \quad (13b)$$

then Eq. (7) recovers the Cahn–Hilliard equation with the second order of accuracy

$$\partial_t \phi + \vec{\nabla} \cdot (\phi \vec{u}) - \theta_M \vec{\nabla}^2 \mu_\phi + O(\delta^2) = 0, \quad (14)$$

where the mobility is defined as

$$\theta_M = q \left(\tau_\phi q - \frac{1}{2} \right) \delta \Gamma. \quad (15)$$

Besides, Eqs. (12) and (13a) also show that they do not require the fourth order isotropic lattice tensor as the conventional lattice Boltzmann Methods need. Thus, D2Q5 is used in this work. That is, the discrete velocities are

$$\vec{c}_1 = (0 \ 0)^T, \quad \vec{c}_{2,4} = (\pm 1 \ 0)^T, \quad \vec{c}_{3,5} = (0 \ \pm 1)^T. \quad (16)$$

According to Eqs. (10)–(13), the equilibrium distribution function in Eq. (8) can be expressed as follows:

$$\mathbf{g}_i^{(0)} = A_i + B_i \phi + C_i \phi \vec{c}_i \cdot \vec{u}. \quad (17)$$

The coefficients are taken as

$$\begin{aligned} B_1 &= 1, \quad B_i = 0 \quad (i \neq 1), \\ C_i &= \frac{1}{2q}, \\ A_1 &= -2\Gamma\mu_\phi, \quad A_i = \frac{1}{2}\Gamma\mu_\phi \quad (i \neq 1), \end{aligned} \quad (18)$$

where Γ is used to control the mobility.

2.2. The continuity and momentum equations

In Eq. (2), the term $\vec{\nabla} \cdot \mathbf{P}$ is related to the surface tension force. This force can be rewritten as a potential term [14,11],

$$\vec{F}_s = -\vec{\nabla} \cdot \mathbf{P} = -\phi \vec{\nabla} \mu_\phi - \vec{\nabla} p_0, \quad (19)$$

where $p_0 = nc_s^2$, c_s is the speed of sound.

The potential form for the surface tension force is adopted to keep the energy conservation. Mathematically, the potential form and the stress form of Eq. (19) are identical. However, numerically, the discretization error is different [11]. Thus, it is useful to eliminate parasite current. It will be discussed later.

As a result, the Navier–Stokes equations can be rewritten as

$$\frac{\partial n}{\partial t} + \vec{\nabla} \cdot (n\vec{u}) = 0, \quad (20)$$

$$\frac{\partial(n\vec{u})}{\partial t} + \vec{\nabla} \cdot (n\vec{u}\vec{u}) = -\vec{\nabla}(p_0 + \phi\mu_\phi) + \mu_\phi \vec{\nabla} \phi + \vec{F}_b + \mu \vec{\nabla}^2 \vec{u}. \quad (21)$$

The chemical potential can be derived from the free energy density functional. We adopt a free energy functional in a closed volume with a mixture of two fluids taking the form [25,14,10]

$$F = \int \mathfrak{F} dV = \int dV \left[\psi(\phi) + \frac{\kappa}{2} (\vec{\nabla} \phi)^2 + \frac{n \ln n}{3} \right]. \quad (22)$$

Here, V is a control volume, κ is a coefficient which is related to the surface tension and the thickness of the interface layer. ψ is the bulk free energy density per unit mass for the homogeneous system. The square of gradient term is associated with variations of the density and contributes to the free energy excess of the interfacial region which defines the surface energy [25]. It is chosen as a double-well form,

$$\psi(\phi) = A(\phi^2 - \phi^{*2})^2. \quad (23)$$

where A is an amplitude parameter to control the interaction energy between the two phases; ϕ is the order parameter. This form will contribute to two equilibrium states, ϕ^* and $-\phi^*$.

We can easily compute the chemical potential as

$$\mu_\phi = \frac{\partial \mathfrak{F}}{\partial \phi} - \vec{\nabla} \cdot \frac{\partial \mathfrak{F}}{\partial \vec{\nabla} \phi} = A(4\phi^3 - 4\phi^{*2}\phi) - \kappa \nabla^2 \phi, \quad (24)$$

and the correspondent pressure tensor as

$$P_{\alpha\beta} = \phi\mu_\phi - \mathfrak{F} = p\delta_{\alpha\beta} - \kappa[(\vec{\nabla} \phi)^2 \delta_{\alpha\beta} - \nabla_\alpha \phi \nabla_\beta \phi], \quad (25)$$

where the pressure is calculated by

$$p = A(3\phi^4 - 2\phi^{*2}\phi^2 - \phi^{*4}) - \kappa \phi \nabla^2 \phi + \frac{(\vec{\nabla} \phi)^2}{2} + \frac{n}{3}. \quad (26)$$

Following the same procedure as [9], we can obtain the profile along the normal direction of the interface

$$\phi = \phi^* \tanh(2\zeta/W), \quad (27)$$

where ζ is the coordinate which is perpendicular to the interface, and W is the thickness of interface layer,

$$W = \frac{\sqrt{2\kappa/A}}{\phi^*}. \quad (28)$$

For a flat interface, the surface tension coefficient can be evaluated by Rowlinson and Widom [25]

$$\sigma = \int \kappa \left(\frac{\partial \phi}{\partial \zeta} \right)^2 d\zeta. \quad (29)$$

From Eqs. (27) and (28), we can obtain the surface tension coefficient as

$$\sigma = \frac{4\sqrt{2\kappa A}}{3} \phi^{*3}, \quad (30)$$

where the expected order parameter is

$$\phi^* = \frac{\rho_H - \rho_L}{2}. \quad (31)$$

Without losing generality, we can easily obtain from Eqs. (24) and (27)

$$\mu_\phi \nabla_\zeta \phi = \frac{3\sigma}{W^2} \tanh^3 \left(\frac{2\zeta}{W} \right) \text{sech}^2 \left(\frac{2\zeta}{W} \right). \quad (32)$$

Thus, the potential form of the surface tension related term is independent of the density and density difference. It is obvious that $\mu_\phi \nabla_\zeta \phi$ is related with the surface tension coefficient and the width of the interface layer. This form of surface tension force is useful for large density ratio. It will also help to reduce the parasite current [11].

The lattice Boltzmann implementation of Eqs. (20) and (21) can be described as

$$f_i(\vec{x} + \vec{c}_i \delta t, t + \delta t) = f_i(\vec{x}, t) + \Omega_i, \quad (33)$$

with

$$\Omega_i = \frac{f_i^{(0)}(\vec{x}, t) - f_i(\vec{x}, t)}{\tau_n} + \left(1 - \frac{1}{2\tau} \right) \frac{w_i}{c_s^2} \left[(\vec{c}_i - \vec{u}) + \frac{(\vec{c}_i \cdot \vec{u})}{c_s^2} \vec{c}_i \right] (\mu_\phi \vec{\nabla} \phi + \vec{F}_b) \delta t. \quad (34)$$

The equilibrium distribution functions satisfy the conservation laws as

$$n = \sum_i f_i^{(0)}, \quad (35)$$

$$\vec{u} = \left(\sum_i f_i^{(0)} \vec{c}_i + \frac{1}{2} (\mu_\phi \vec{\nabla} \phi + \vec{F}_b) \right) / n, \quad (36)$$

$$\sum_i f_i^{(0)} c_{ix} c_{i\beta} = (\phi \mu_\phi + c_s^2 n) \delta_{x\beta} + n u_x u_\beta. \quad (37)$$

Note that the force terms are incorporated in Eqs. (34) and (36) [5]. By using the Taylor series expansion to the second order, Eq. (33) can be rewritten as

$$\delta(\partial_t + \vec{c}_i \cdot \nabla) f_i + \frac{1}{2} \delta^2 (\partial_t + \vec{c}_i \cdot \nabla)^2 f_i + O(\delta^3) = \Omega_i. \quad (38)$$

And Using the Chapman–Enskog expansion to Eq. (38),

$$\begin{aligned} f_i &\approx f_i^{(0)} + \varepsilon f_i^{(1)} + \varepsilon^2 f_i^{(2)}, \\ \partial_t &\approx \varepsilon \partial_{t^0} + \varepsilon^2 \partial_{t^1}, \\ \partial_x &\approx \varepsilon \partial_{x^1}. \end{aligned} \quad (39)$$

According to Eqs. (35)–(37), we can approximately recover the governing equations to the second order

$$\begin{aligned} \frac{\partial(nu_x)}{\partial t} + \partial_\beta(nu_x u_\beta) = & -\nabla_\alpha \Phi + (\mu_\phi \vec{\nabla} \phi + \vec{F}_b) + \partial_\beta[\mu(\partial_\alpha u_\beta + \partial_\beta u_\alpha)] + (c_s^2 - \partial_n \Phi) \partial_\gamma(\rho u_\gamma) \delta_{\alpha\beta} \\ & + (c_s^2 - \partial_n \Phi)[u_\alpha \partial_\beta n + u_\beta \partial_\alpha n] - \partial_\gamma(nu_x u_\beta u_\gamma) \end{aligned}$$

with

$$\Phi = \phi \mu_\phi + c_s^2 n$$

and

$$\mu = c_s^2(\tau_n - 0.5)n.$$

The term $\partial_\gamma(nu_x u_\beta u_\gamma)$ is also appeared in the standard LBM. This higher order derivative term is quite small and can be neglected. Because ϕ is an independent variable to n and μ_ϕ is only a function of ϕ , we can obtain $\partial_n \Phi = c_s^2$. Thus, the second line in the above equation is negligible, and we can approximately recover the governing equations (20) and (21).

From Eqs. (35)–(37), we can construct the correspondent equilibrium distribution functions (based on D2Q9) as

$$f_i^{(0)} = w_i A_i + w_i n \left(3c_{ix} u_x - \frac{3}{2} u^2 + \frac{9}{2} u_x u_\beta c_{ix} c_{i\beta} \right), \quad (40)$$

where the coefficients are taken as

$$\begin{aligned} A_1 &= \frac{9}{4} n - \frac{15(\phi \mu_\phi + \frac{1}{3} n)}{4}, \quad A_i|_{i=2,\dots,9} = 3 \left(\phi \mu_\phi + \frac{1}{3} n \right), \\ w_1 &= \frac{4}{9}, \quad w_i|_{i=2,\dots,5} = \frac{1}{9}, \quad w_i|_{i=6,\dots,9} = \frac{1}{36}. \end{aligned} \quad (41)$$

To include the buoyancy force, we add the additional term δf_i and δg_i to Eqs. (33) and (7) respectively as did by Takada et al. [31].

3. Numerical validation

3.1. A bubble in the stationary flow

The 2D stationary bubble is a benchmark test to verify various models for multiphase flows. Initially, a circular bubble is located at the center of a domain. The periodic boundary condition is employed at all boundaries. The density ratio is set to be 1000 ($\rho_H = 1000$, $\rho_L = 1$), which is correspondent to the initial order parameter, $\phi^* = 499.5$. At beginning, the order parameter is set to be ϕ^* inside the bubble and $-\phi^*$ elsewhere. The parameters are fixed as $\sigma = 0.1$ and $\Gamma = 100$. The relaxation times are $\tau_n = 0.875$ and $\tau_\phi = 0.7$.

We know that Laplace law for the two-dimensional case is

$$\Delta p = \frac{\sigma}{R}, \quad (42)$$

where Δp is the pressure jump across the interface. R is the radius of the bubble. For the numerical computation, we first fix the mesh size as 120×120 , and investigate the influence of the thickness of the interface layer. The radius is set to be half of the height. The width of the interface layer is taken as 2, 3, 3.5, 4, 4.5, 5 and 5.5. Like other numerical methods, the pressure is calculated as an average value at grid points that are away from the interface of the bubble. Then, the numerical results of the surface tension can be calculated from Eq. (42). The numerical results and the analytical solution (Eq. (30)) are drawn as a function of the width of the interface layer in Fig. 1. It can be seen clearly that the numerical solution approaches the analytical solution as the thickness of the interface layer increases. When the thickness of the interface layer is bigger than 4.5, the numerical result changes very little and matches the analytical value. This is due to the fact that the discretization error decreases with the thickness of the interface layer [18]. In this case, the spurious current

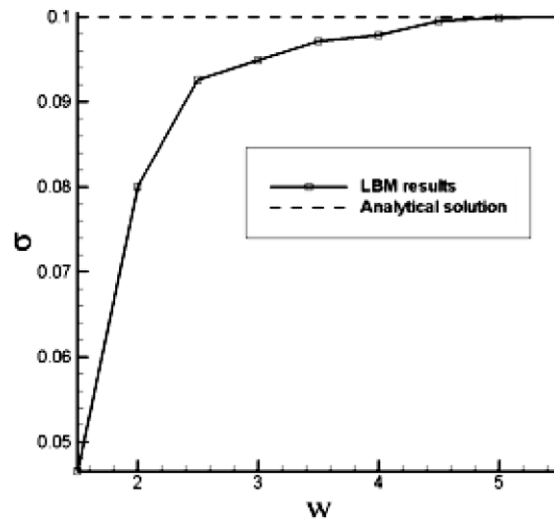


Fig. 1. The influence of the width of the interface layer.

can go down to 10^{-9} and even smaller. In fact, the spurious current is influenced by the thickness of the interface layer and the surface tension coefficient. A large width of the interface layer and small surface tension coefficient will reduce the spurious current.

To verify the Laplace law, we fix the thickness of the interface layer to be 5 and change the radius of bubble R from 20 to 200. Accordingly, the width and height of the domain are set as 800 respectively. As discussed above, the average pressure inside the bubble and outside the bubble is calculated to obtain the pressure jump. The pressure jump is plotted as a function of the curvature in Fig. 2. It can be easily observed that like the work of Kang et al. [13], the relationship is linear as the Laplace law. Besides, the slope also agrees well with the analytical solution (surface tension). These show that the Laplace law is accurately satisfied. Eq. (27) can also be applied to this case to verify the accuracy of numerical results. It can be written as

$$\phi = \phi^* \tanh \left(2 \frac{\sqrt{(x - x_c)^2 + (y - y_c)^2} - R}{W} \right), \quad (43)$$

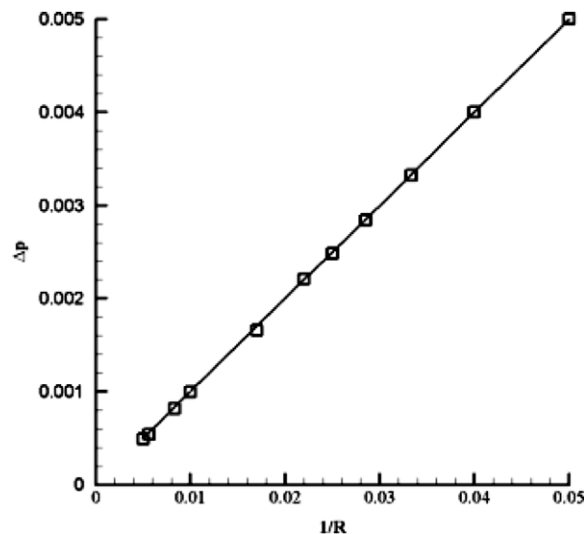


Fig. 2. The verification of Laplace law.

where x_c and y_c are the coordinates of the center of the bubble. We can fix the width of the interface layer and the mesh size as 4.5 and 120×120 respectively. Fig. 3 displays the order parameter at all lattice points as a function of the distance from the center point. All data points lie on the analytical curve as shown in Eq. (43). That is, it is independent of the direction. The figure shows that the flow is isotropic.

3.2. Effect of mobility coefficient Γ and width of interface layer

To study the effect of mobility coefficient Γ and the width of interface layer on the numerical results, we consider two stationary bubbles without collision. The computational domain is taken as 120×120 . Initially, two circular bubbles with the radius R are located horizontally with a gap of d . The periodic boundary condition is employed at all boundaries. The density ratio is set as 1000 with $\rho_H = 1000$, $\rho_L = 1$. The parameters are chosen as $R = 20$, $\sigma = 1$, $\tau_n = 0.6$, $\tau_\phi = 0.7$. The gap of the two bubbles (d) is taken as 5, while the width of the interface (w) and the mobility coefficient Γ are varied.

For the two stationary bubbles without collision, it was found that the distance (gap) between the bubbles and the interface width (w) are the major factors to decide whether the two bubbles will merge together or not. When the gap of the two bubbles is larger than $2w$, the two bubbles will not merge. Otherwise, they will merge together. In the later case, a larger mobility coefficient Γ makes the two bubbles merge together more quickly.

At first, we set the width of the interface layer as $w = 2.4$, and $\Gamma = 40$. That is, the gap of two bubbles is larger than $2w$. Numerical results are shown in Fig. 4. It can be easily observed that the two bubbles do not merge at any time. When we set a larger value of $\Gamma = 400$ and remain the interface width as 2.4, the numerical results are the same as shown above. In fact, even when the interface width is set as 2.5, the two bubbles do not merge together. Based on the numerical results, we may draw a conclusion that the two bubbles will not merge when their gap is larger than twice the interface width.

Next, the interface width is set as $w = 2.6$ and the Γ value is remained as 400. This is the case where the gap of two bubbles is less than $2w$. The other parameters remain unchanged. The results are shown in Fig. 5. It can be easily observed that the two bubbles merge eventually without collision. To show the effect of mobility coefficient Γ on the numerical results, the interface width is remained as $w = 2.6$ and the Γ value is reduced to 40. The other parameters remain unchanged. The results are shown in Fig. 6. It can be seen clearly that the two bubbles merge without collision. However, the merging process is much slower than the case where the Γ value is 400. Besides, there is an oscillation process occurring during the merging process.

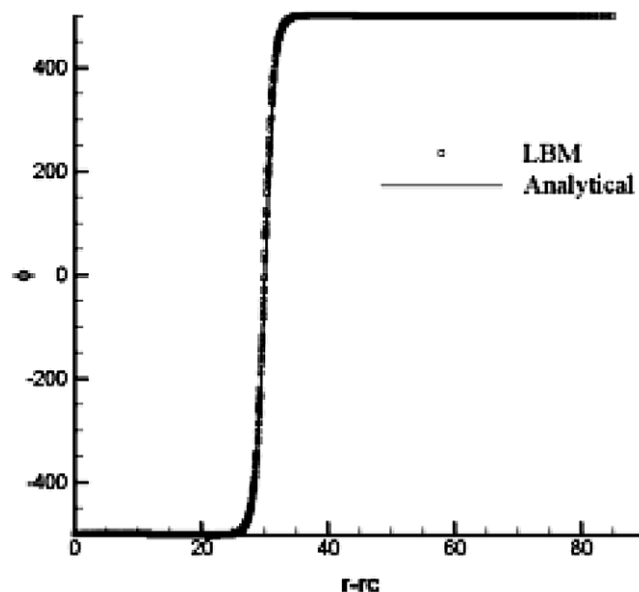


Fig. 3. The interface profile.

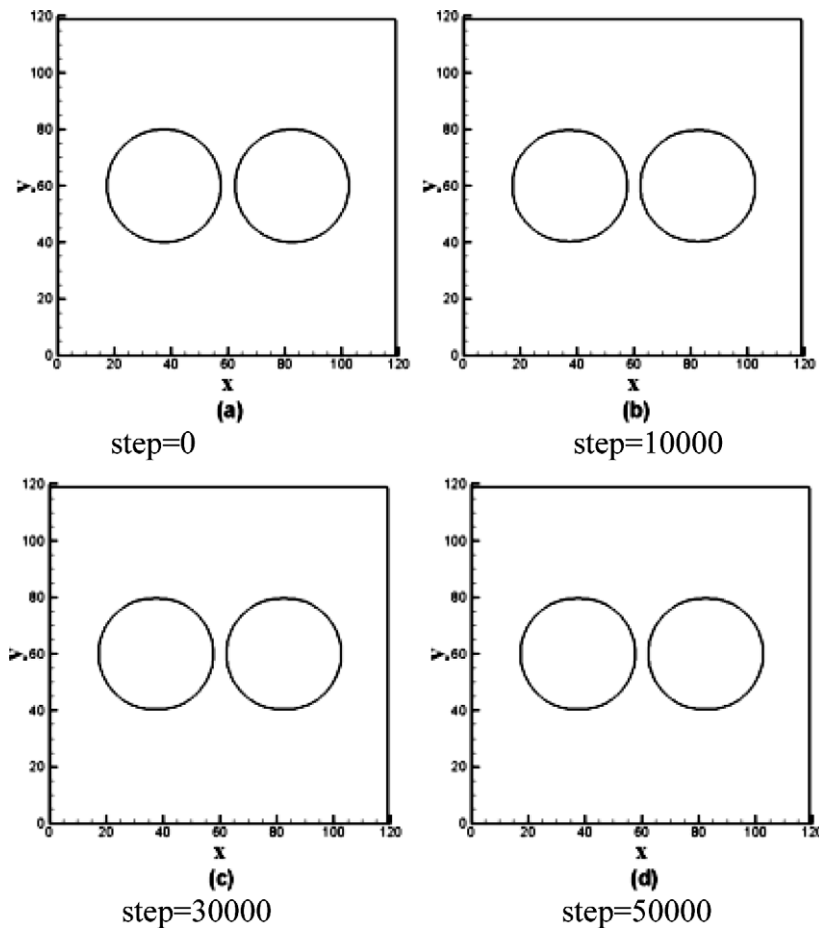


Fig. 4. Results of two stationary bubbles without collision ($w = 2.4$, $d_{\text{int}} = 5$, $\Gamma = 40$).

The above numerical results demonstrate that the Γ value should be chosen as small as possible for practical applications. On the other hand, very small value of Γ will cause numerical instability. So, we have to balance these two factors.

3.3. Capillary wave

The capillary wave is another test case used to validate the numerical approach. As we know, if a plane interface is deformed in a wave-like manner, the positive and negative pressure will be posed on different sides of the interface. Under the influence of surface tension and viscous forces, the system will damp to the equilibrium state. If the wave amplitude is not very large, it could be approximately modeled by the sub-linear theory [22,17]. Here, the order parameters are initialized as a sinusoidal curve around $y = NY/2$ of one wavelength NX ,

$$\phi = \phi^* \tanh \left[2 \left(y - \frac{NY}{2} - a \sin \kappa_w x \right) / W \right], \quad (44)$$

where a is the initial amplitude

$$\frac{a}{NY} = 0.02, \quad (45)$$

and κ_w is the wave number

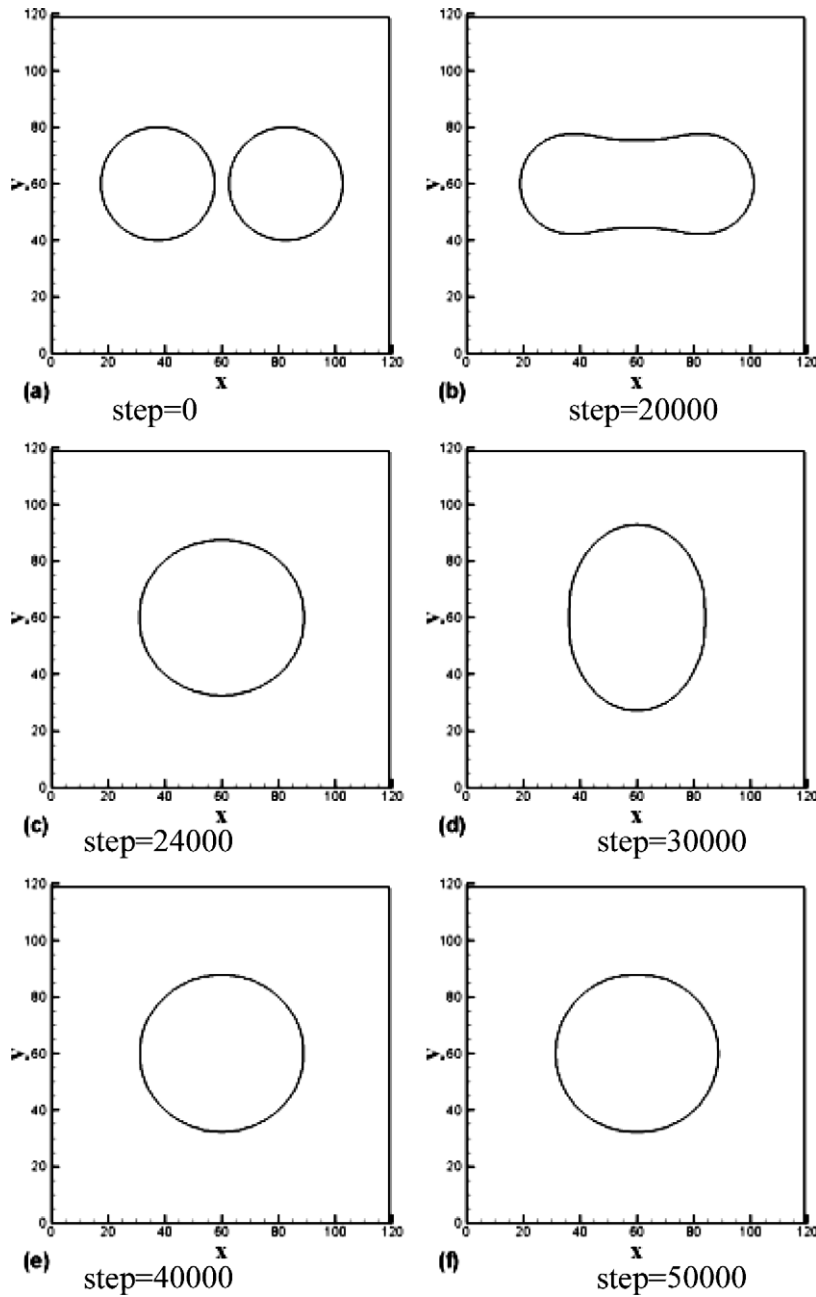


Fig. 5. Results of two stationary bubbles without collision ($w = 2.6$, $d_{\text{int}} = 5$, $\Gamma = 400$).

$$\kappa_w = \frac{2\pi}{\lambda} = \frac{2\pi}{NX}. \quad (46)$$

Here, NX and NY are the width and height of the domain.

As the interface is damped and oscillates with time, the oscillating period should not be too long before the wave is damped out so that we can capture the capillary wave. Non-slip boundary condition is employed on both the upper and lower walls. The boundary condition in the x -direction is periodic. The same viscosity is used in the two phases. At each time step, at a certain x -value, the height of interface is measured. Since the position of the interface may not lie at the grid point, it is calculated by interpolation,

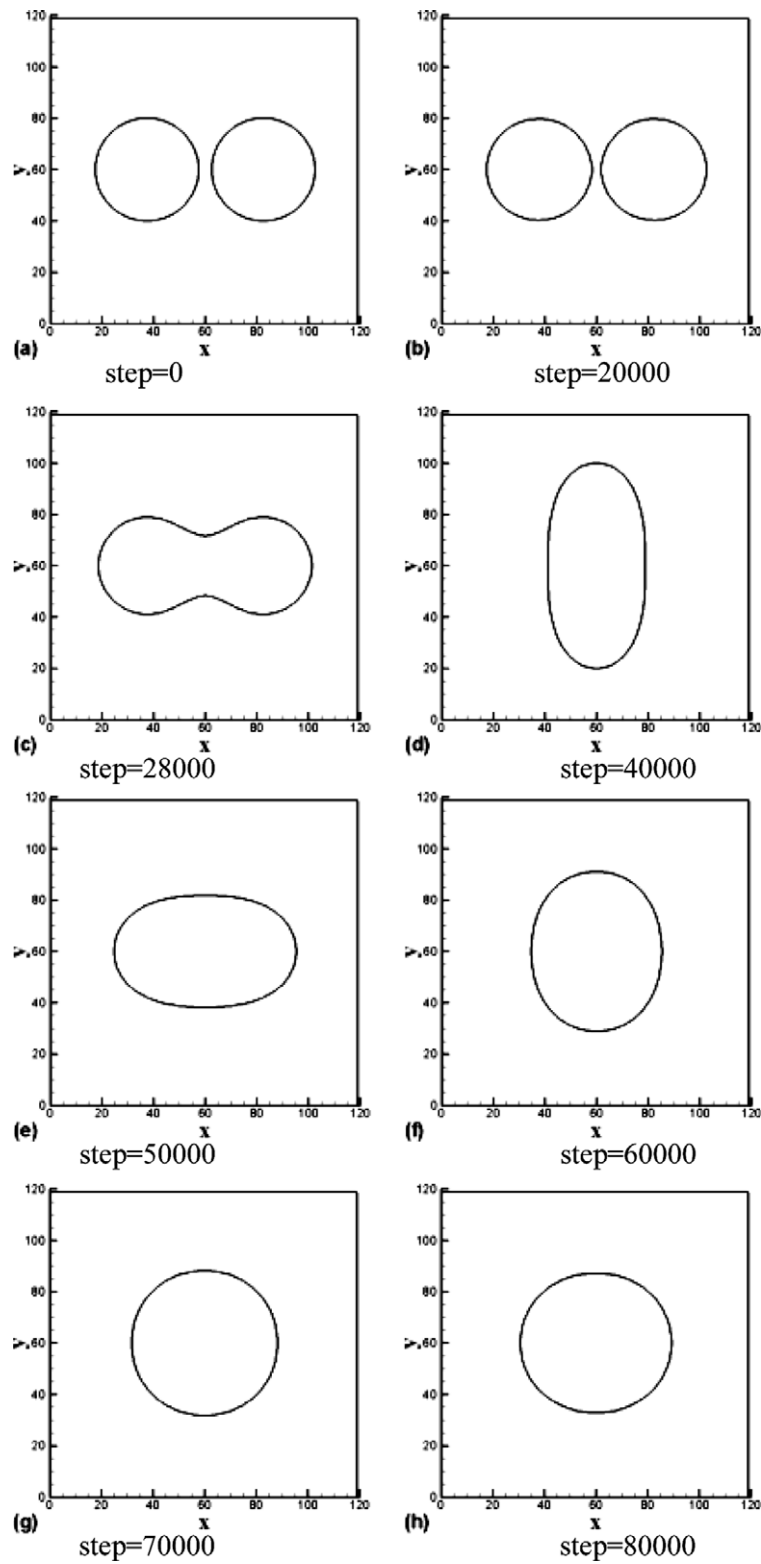


Fig. 6. Results of two stationary bubbles without collision ($w = 2.6$, $d_{\text{int}} = 5$, $\Gamma = 40$).

$$y = iy - \frac{\phi(iy)}{\phi(iy) - \phi(iy - 1)}, \quad \text{where } \phi(iy)\phi(iy - 1) < 0. \quad (47)$$

This curve is used to find the oscillation frequency of the wave. The oscillation frequency from the theory [22,12] is

$$\omega = \sqrt{\frac{\sigma \kappa_w^3}{\rho_H + \rho_L}}. \quad (48)$$

The parameters are taken as $\rho_H = 1000$, $\rho_L = 1$, $\sigma = 0.521$, $\tau_n = 0.6$, $\tau_\phi = 0.7$, $\Gamma = 100$, $a/NY = 0.02$, $W = 5$. We only change the number of grid points in X direction (NX) from 32 to 128. This is equivalent to change the wave number. From the position of interface, which oscillates and damps with time, we can measure the time difference between the neighboring peak points, and calculate the oscillation period. Thus, the numerical angular frequency can be obtained. These angular frequencies are listed in Table 1. It can be easily observed that the angular frequencies are increased as the wave number increases. The obtained numerical values agree well with the theoretic results given by Eq. (48). Besides, the numerical value of angular frequency approaches the theoretical value when the ratio NX/NY is small. This is the assumption of the linear theory [17].

3.4. Bubble rising under buoyancy

In this section, the two-dimensional single bubble rising under buoyancy is simulated. The density of each phase and the surface tension coefficient are taken the same as those used by Takada et al. [31],

$$\rho_H = 1.42, \quad \rho_L = 0.58, \quad \sigma = 0.00521, \quad (49)$$

The bubble is surrounded with stationary walls. Initially, it is located at the lower region (one fourth of the height) of computational domain of 80×300 . The initial order parameter is set to be ϕ^* inside the bubble and $-\phi^*$ elsewhere. Several simulations are performed under different parameters as shown in Table 2. As the radius of the bubble is quite small, we should not set the thickness of the interface layer to be too large.

The dimensionless parameters (Eotvos and Morton number) are defined as [31]

$$Eo = \frac{g(\rho_H - \rho_L)d^2}{\sigma}, \quad M = \frac{g(\rho_H - \rho_L)\mu_H^4}{\rho_H^2\sigma^3}, \quad Re = \frac{\rho_H V_T d}{\mu_H}. \quad (50)$$

The bubble will rise at a nearly constant velocity as the balance between the buoyancy and drag force. In fact, this velocity is not a constant. There are some oscillations during the rising process. The bubble velocity is calculated by

$$\vec{V}_{\text{bubble}} = \frac{\sum_x \phi \vec{V}}{\sum_x \phi}, \quad \text{where } \phi < 0. \quad (51)$$

The comparisons of simulation results are shown in Table 3. It can be easily observed that they agree very well with those of VOF method and Takada's LBM (2001). As shown in Table 2, the Eotvos number, Eo , gradually

Table 1
The angular frequency of capillary wave

Cases	Mesh	ω (present)	ω (theory)
1	32×256	2.01e−3	2.00e−3
2	64×256	7.06e−4	7.02e−4
3	128×256	2.37e−4	2.48e−4

Table 2
Parameters for the simulation of a bubble rising under buoyancy

Cases	Eo	M	W
1	5	0.2267	3
2	10	0.4535	3
3	20	0.9070	2
4	40	1.8134	1.5

Table 3
Terminal velocity of a bubble rising under buoyancy

Cases	Vt (present)	Vt (VOF)	Vt (Takada)
1	8.02e−3	8.28e−3	7.82e−3
2	1.44e−2	1.43e−2	1.38e−2
3	2.14e−2	2.15e−2	2.17e−2
4	3.20e−2	3.08e−2	3.11e−2

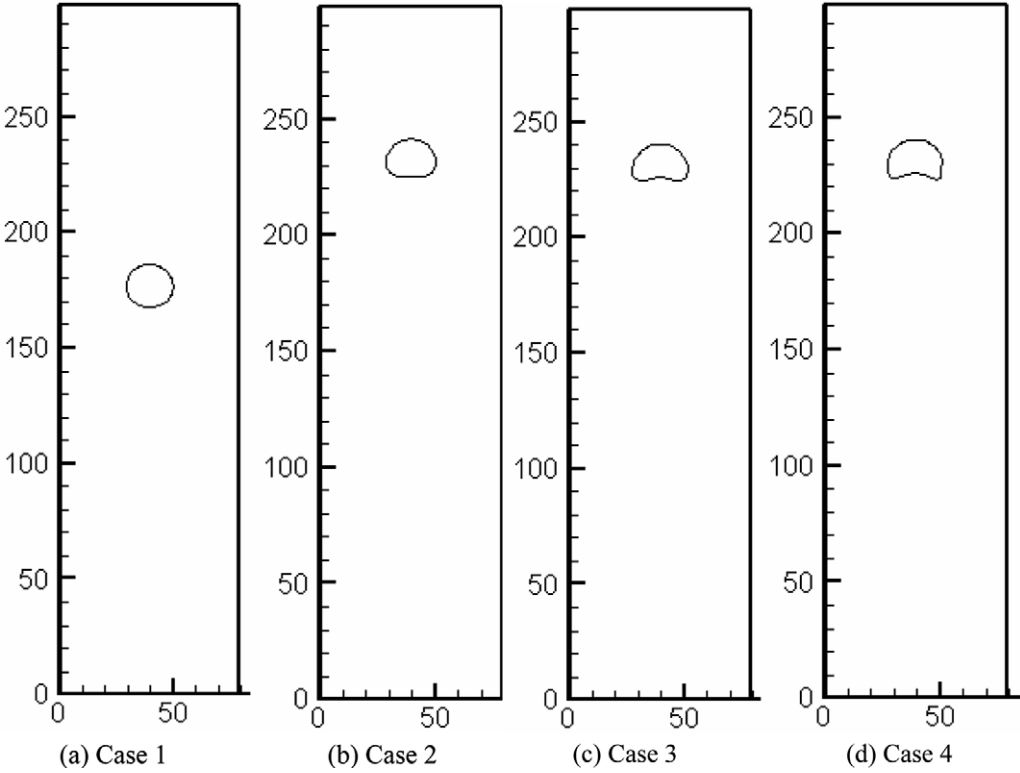


Fig. 7. Bubble shapes under different conditions.

increases from 5 of Case 1 to 40 of Case 4. Eq. (50) indicates that the increase of Eo is equivalent to the decrease of the surface tension coefficient σ . It is well known that the surface tension force is to resist the deformation of the bubble. In other words, the decrease of σ will enhance the deformation of the bubble. This phenomenon is clearly revealed in Fig. 7, which displays the bubble shape of 4 cases. The bubble of Case 1 is very close to the original shape (circle). As Eo increases, the bubble shape deforms more and more from Case 2 to Case 4. In terms of the bubble shapes, the present results are very similar to those of Takada’s method (2001).

Next, we apply the present method to simulate a real bubble rising case with large density ratio. Initially, a bubble with the radius of 20 is located inside the domain of 120×240 . The center of the bubble is (60, 60). The densities and surface tension force coefficient are set as

$$\rho_H = 1000, \quad \rho_L = 1, \quad \sigma = 2, \quad \Gamma = 100.$$

Four cases are considered for the numerical simulation. The respective Eotvos numbers of the four cases are 15.984, 39.96, 79.92 and 239.76. Accordingly, the Morton numbers of the four cases are 0.6097, 1.52425, 3.0485 and 9.146 and the Reynolds numbers are 3.2, 5.984, 9.12 and 16. The typical flow patterns of the four cases are shown in Figs. 8–11, where the red curves¹ represent the bubble shapes (interfaces), which are defined

¹ For interpretation of color in Figs. 8–11, the reader is referred to the web version of this article.

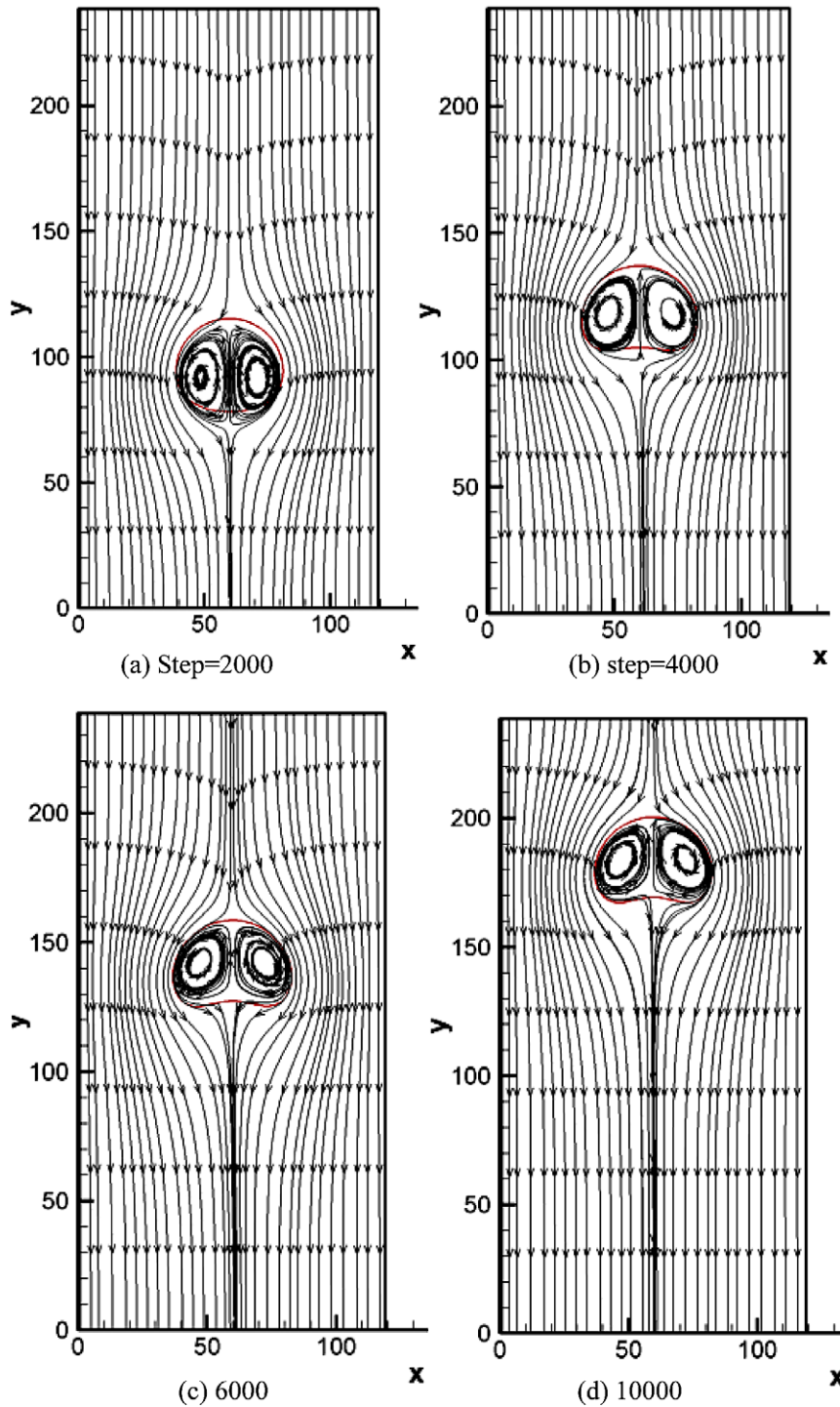


Fig. 8. The flow pattern of a bubble rising under buoyancy with density ratio of 1000 ($Eo = 15.9840$, $M = 0.6097$, $Re = 3.2$).

as the position where the order parameter is zero. From these figures, it can be easily observed that the four representative bubble shapes are disc, spherical cap, spherical cap and skirt respectively. These shapes are in line with the experimental findings [1]. For all the cases, a pair of vortex is first formed inside the bubble at

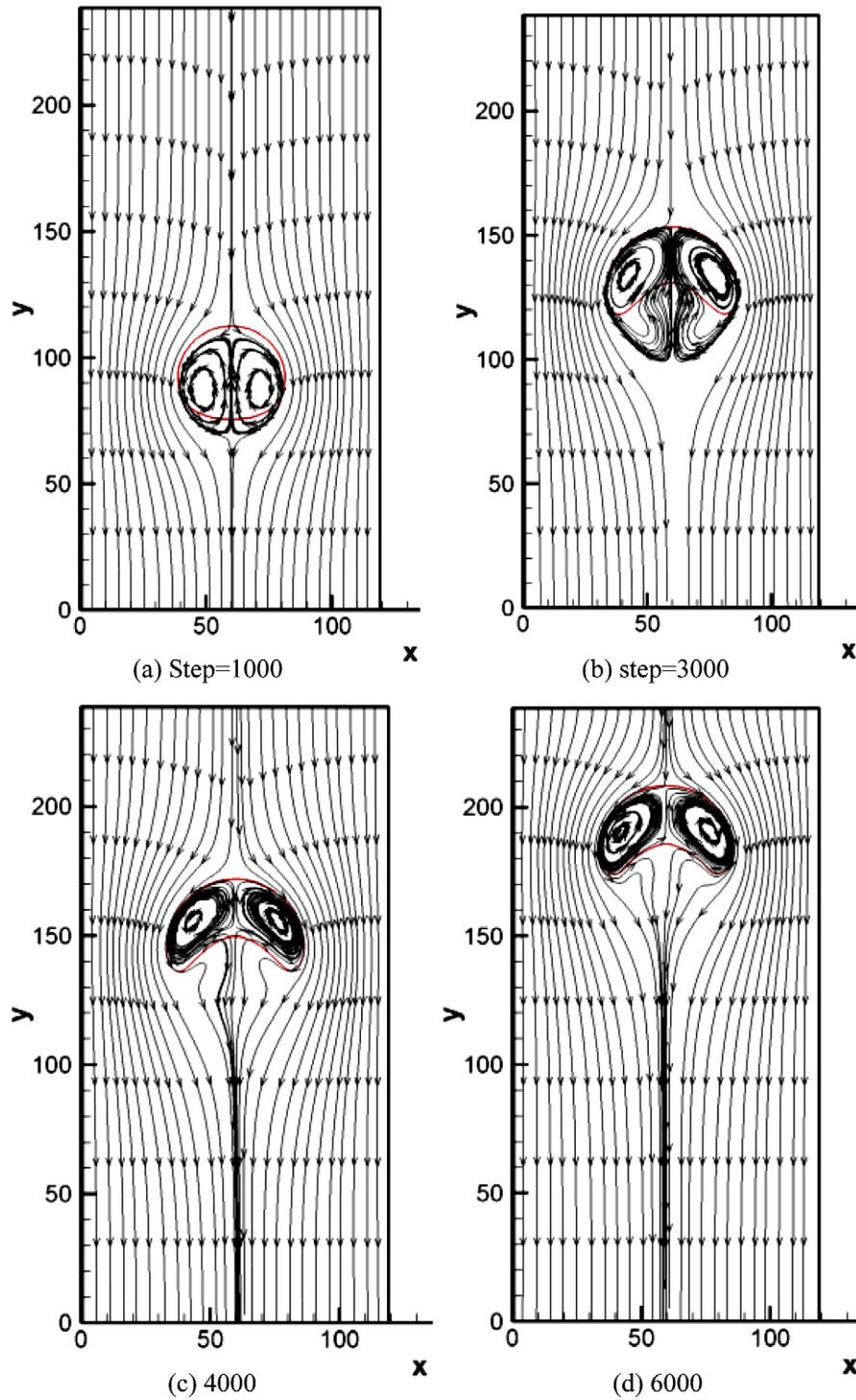


Fig. 9. The flow pattern of a bubble rising under buoyancy with density ratio of 1000 ($Eo = 39.96$, $M = 1.52425$, $Re = 5.984$).

beginning. Due to buoyancy force, the bubble will move upwards. In the meantime, the middle part of the bubble will encounter a larger deformation due to the hit of surrounding water. When $Eo = 15.984$, the shape of the bubble does not change too much. This is because for this case, the surface tension force is very strong,

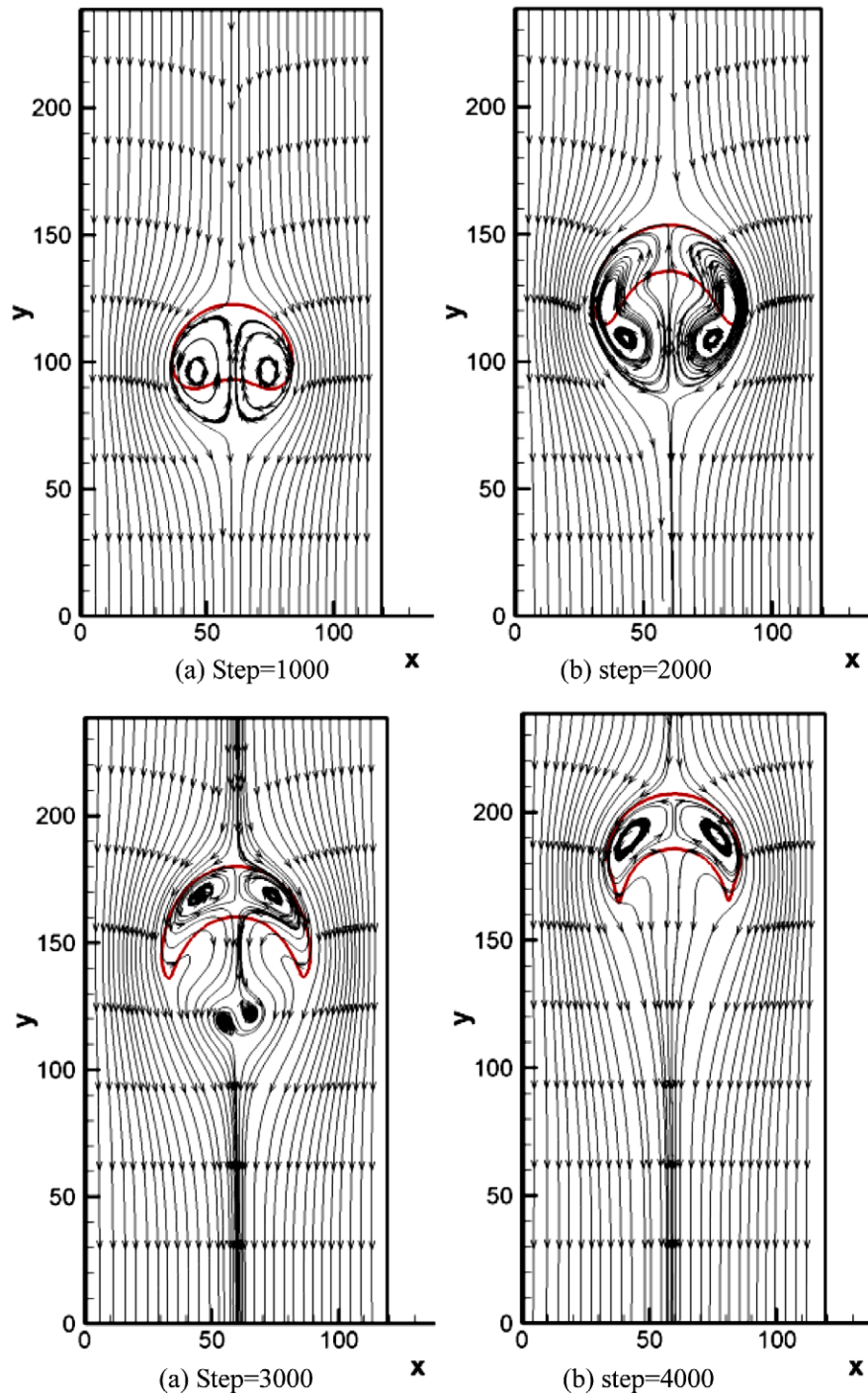


Fig. 10. The flow pattern of a bubble rising under buoyancy with density ratio of 1000 ($Eo = 79.92$, $M = 3.0485$, $Re = 9.12$).

trying to keep its original configuration. As shown in Figs. 9–11, when Eo increases (surface tension force decreases), the bubble moves up faster and faster, and the bubble shape changes greatly. Accordingly, the flow patterns become more complex. For all the cases, the bubble is always kept symmetric, and a wake flow is developed behind the bubble.

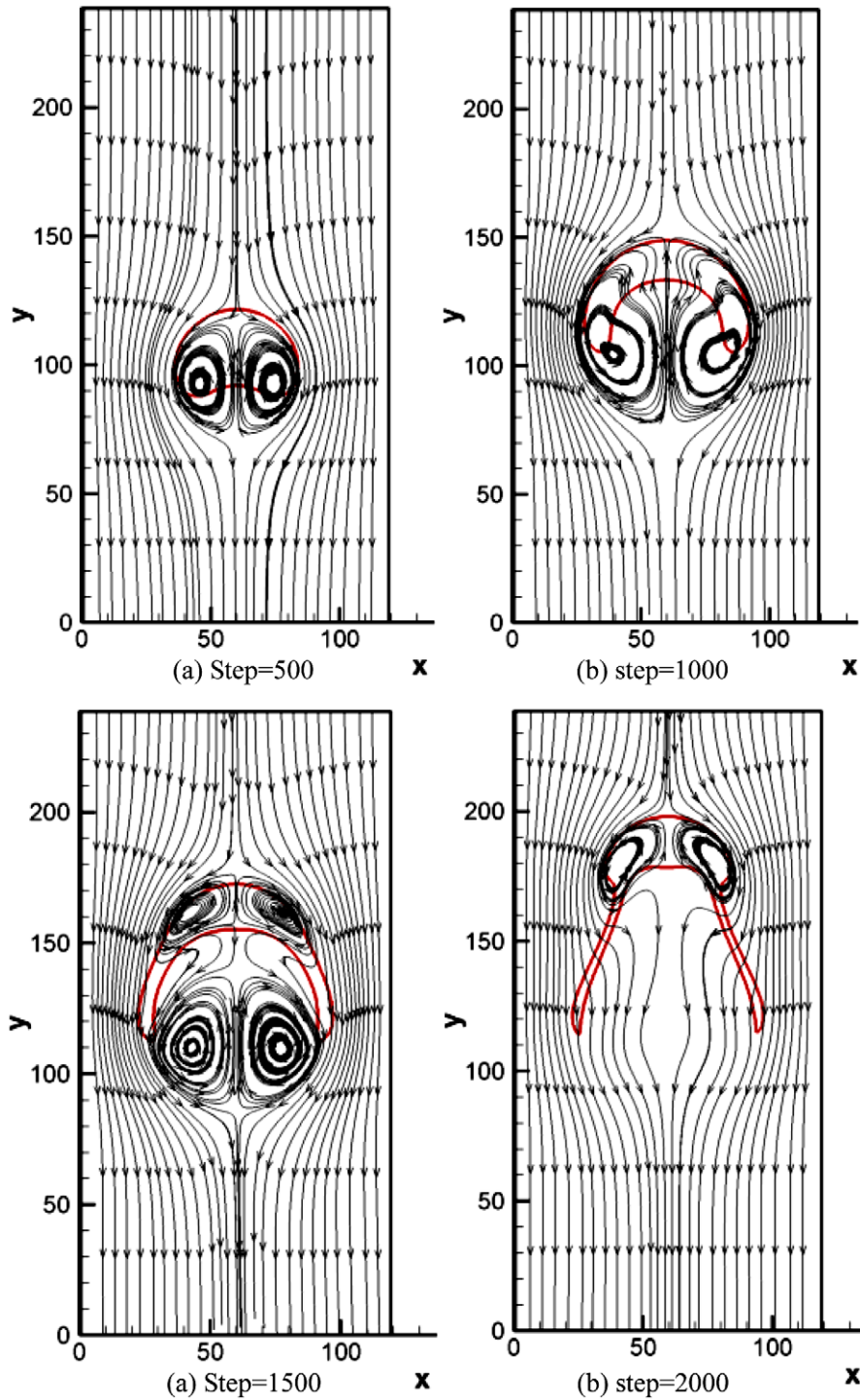


Fig. 11. The flow pattern of a bubble rising under buoyancy with density ratio of 1000 ($Eo = 239.76$, $M = 9.146$, $Re = 16$).

4. Conclusions

A lattice Boltzmann model for multiphase flows with high density ratio is developed in this paper. It can be easily implemented, and does not require pressure correction as needed by Inamuro et al. [8] and any complex

discretization as needed by Lee and Lin [18]. Several numerical verifications are applied to validate the approach. Numerical results show that the proposed approach satisfies the Laplace law. Besides, the numerical angular frequency of capillary wave with large density ratio agrees well with the theoretical prediction. The present results agree well with numerical data of Takada et al. [31] and the experimental findings of Bhaga and Weber [1] for a real bubble rising under buoyancy with density ratio of 1000. It is indicated that the extension of present work to three-dimensional case is straightforward. The interface capturing equation only needs 7 bit velocity model. This will greatly improve the efficiency. For the three-dimensional work, we will report it in the following paper.

References

- [1] D. Bhaga, M.E. Weber, Bubbles in viscous liquids: shapes, wakes and velocities, *J. Fluid Mech.* 105 (1981) 61–85.
- [2] P. Bhatnagar, E.P. Gross, M.K. Krook, A model for collision processes in gases, *Phys. Rev.* 94 (1954).
- [3] J.W. Cahn, J.E. Hilliard, Free energy of a nonuniform system. I. Interfacial energy, *J. Chem. Phys.* 28 (2) (1958) 258–267.
- [4] S. Chen, G. Doolen, Lattice Boltzmann method for fluid flows, *Annu. Rev. Fluid Mech.* 30 (1998) 329–364.
- [5] Z. Guo, C. Zhen, B. Shi, Discrete lattice effects on the forcing term in the lattice Boltzmann method, *Phys. Rev. E* 65 (4) (2002) 046308.
- [6] X. He, S. Chen, R. Zhang, A lattice Boltzmann scheme for incompressible multiphase flow and its application in simulation of Rayleigh–Taylor instability, *J. Comput. Phys.* 152 (2) (1999) 642–663.
- [7] C.W. Hirt, B.D. Nichols, Volume of fluid (VOF) methods for the dynamics of free boundaries, *J. Comput. Phys.* 39 (1981) 201–225.
- [8] T. Inamuro, T. Ogata, S. Tajima, N. Konishi, A lattice Boltzmann method for incompressible two-phase flows with large density differences, *J. Comput. Phys.* 198 (2004) 628–644.
- [9] D. Jacqmin, Calculation of two-phase Navier–Stokes flows using phase-field modeling, *J. Comput. Phys.* 155 (1999) 96–127.
- [10] D. Jamet, O. Lebaigue, N. Coutris, J.M. Delhay, The second gradient method for the direct numerical simulation of liquid–vapor flows with phase change, *J. Comput. Phys.* 169 (2001) 624–651.
- [11] D. Jamet, D. Torres, J.U. Brackbill, On the theory and computation of surface tension: the elimination of parasitic currents through energy conservation in the second-gradient method, *J. Comput. Phys.* 182 (2002) 262–276.
- [12] Junseok Kim, A continuous surface tension force formulation for diffuse-interface models, *J. Comput. Phys.* 204 (2) (2005) 784–804.
- [13] Q. Kang, D. Zhang, Shiyi Chen, Displacement of a two-dimensional immiscible droplet in a channel, *Phys. Fluids* 14 (2002) 3023.
- [14] V.M. Kendon, M.E. Cates, I. Pagonabarraga, J.-C. Desplat, P. Bladon, Inertial effects in three-dimensional spinodal decomposition of a symmetric binary fluid mixture: a lattice Boltzmann study, *J. Fluid Mech.* 440 (2001) 147–203.
- [15] A. Lamura, G. Gonnella, Lattice Boltzmann simulations of segregating binary fluid mixtures in shear flow, *Physica A* 294 (2001) 295–312.
- [16] A. Lamura, S. Succi, A lattice Boltzmann for disordered fluids, *Int. J. Mod. Phys. B* 17 (2003) 145–148.
- [17] K. Langaas, J.M. Yeomans, Lattice Boltzmann simulation of a binary fluid with different phase viscosities and its application to fingering in two dimensions, *Eur. Phys. J. B* 15 (2000) 133–141.
- [18] T. Lee, C.-L. Lin, A stable discretization of the lattice Boltzmann equation for simulation of incompressible two-phase flows at high density ratio, *J. Comput. Phys.* 206 (2005) 16–47.
- [19] D. Lorstad, L. Fuchs, High-order surface tension VOF-model for 3D bubble flows with high density ratio, *J. Comput. Phys.* 200 (2004) 153–176.
- [20] S. Osher, J. Sethian, Fronts propagating with curvature dependent speed: algorithms based on Hamilton–Jacobi formulation, *J. Comput. Phys.* 79 (1988) 12–49.
- [21] J.E. Pilliod Jr., E.G. Puckett, Second-order volume-of-fluid algorithms for tracking material interfaces, *J. Comput. Phys.* 199 (2004) 465–502.
- [22] A. Prosperetti, Motion of two superposed viscous fluids, *Phys. Fluids* 24 (1981) 1217–1223.
- [23] W.J. Rider, B.D. Kothe, Reconstructing volume tracking, *J. Comput. Phys.* 141 (1998) 112–152.
- [24] D.H. Rothman, J.M. Keller, Immiscible cellular-automaton fluids, *J. Statist. Phys.* 52 (1988) 1119–1127.
- [25] J.S. Rowlinson, B. Widom, *Molecular Theory of Capillarity*, Clarendon, Oxford, 1989.
- [26] M. Rudman, A volume-tracking method for incompressible multifluid flows with large density variations, *Int. J. Numer. Methods Fluids* 28 (1998) 357–378.
- [27] M. Sussman, E. Fatemi, P. Smereka, S. Osher, An improved level set method for incompressible two-phase flows, *Comput. Fluids* 27 (1998) 663–680.
- [28] X. Shan, H. Chen, Lattice Boltzmann model for simulating flows with multiple phases and components, *Phys. Rev. E* 47 (3) (1993) 1815–1819.
- [29] M.R. Swift, W.R. Osborn, J.M. Yeomans, Lattice Boltzmann simulation of non-ideal fluids, *Phys. Rev. Lett.* 75 (1995) 830–833.
- [30] M.R. Swift, W.R. Osborn, J.M. Yeomans, Lattice Boltzmann simulation of liquid–gas and binary fluid systems, *Phys. Rev. E* 54 (1996) 5041–5052.
- [31] N. Takada, M. Misawa, A. Tomiyama, S. Hosokawa, Simulation of bubble motion under gravity by Lattice Boltzmann Method, *J. Nucl. Sci. Technol.* 38 (5) (2001) 330–341.
- [32] O. Ubbink, R.I. Issa, A method for capturing sharp fluid interfaces on arbitrary meshes, *J. Comput. Phys.* 153 (1999) 26–50.